POLITECNICO DI TORINO
Repository ISTITUZIONALE

Pressure weakens coupling strength in In and Sn elemental superconductors

Original
Pressure weakens coupling strength in In and Sn elemental superconductors / Ummarino, Giovanni Alberto; Khasanov, Rustem. - In: PHYSICAL REVIEW. B. - ISSN 2469-9969. - 110:(2024). [10.1103/PhysRevB.110.214515]

Availability:
This version is available at: 11583/2995778 since: 2024-12-20T17:17:58Z

Publisher:
American Physical Society

Published
DOI:10.1103/PhysRevB.110.214515

Terms of use:

This article is made available under terms and conditions as specified in the corresponding bibliographic description in the repository

Publisher copyright

(Article begins on next page)

05 February 2025

Pressure weakens coupling strength in In and Sn elemental superconductors

Rustem Khasanov [1,*] and Giovanni A. Ummarino [2,3,†]

[1] *PSI Center for Neutron and Muon Sciences CNM, 5232 Villigen PSI, Switzerland*

[2] *Istituto di Ingegneria e Fisica dei Materiali, Dipartimento di Scienza Applicata e Tecnologia, Politecnico di Torino, Corso Duca degli Abruzzi 24, 10129 Torino, Italy*

[3] *National Research Nuclear University MEPhI (Moscow Engineering Physics Institute), Kashira Hwy 31, Moscow 115409, Russia*

(Received 25 August 2024; revised 31 October 2024; accepted 6 December 2024; published 20 December 2024)

The pressure dependence of the thermodynamic critical field B_c in elemental indium (In) and tin (Sn) superconductors was studied by means of muon-spin rotation/relaxation. Pressure enhances the deviation of $B_c(T)$ from the parabolic behavior expected for a typical type-I superconductor, suggesting a weakening of the coupling strength $\alpha = \langle\Delta\rangle/k_B T_c$ ($\langle\Delta\rangle$ is the average value of the superconducting energy gap, T_c is the transition temperature, and k_B is the Boltzmann constant). As pressure increases from 0.0 to $\simeq 3.0$ GPa, α decreases linearly, approaching the limiting weak-coupling Bardeen-Cooper-Schrieffer (BCS) value $\alpha_{BCS} \simeq 1.764$. Analysis of the data within the framework of Eliashberg theory reveals that only part of the pressure effect on α can be attributed to the hardening of the phonon spectra, reflected by a decrease in the electron-phonon coupling constant. Nearly 40% of the effect is caused by an increased anisotropy of the superconducting energy gap.

DOI: 10.1103/PhysRevB.110.214515

I. INTRODUCTION

Pressure is known to be one of the important parameters in superconductor physics. It enables the discovery of many new materials that do not superconduct or may not even exist under ambient pressure conditions but exhibit significantly high critical temperatures under applied pressure [1–3]. In particular, pressure experiments have enabled the discovery of completely new classes of high-temperature superconducting materials, with transition temperatures exceeding the liquid nitrogen level, such as nickelates [4], or even approaching room temperature, such as hydrides [5–7]. At the same time, pressure serves as a clean tuning parameter that, without causing structural changes, fine tunes the crystal lattice and, as a consequence, allows tracking the corresponding changes in various superconducting properties of the material.

In most conventional phonon-mediated superconductors, the application of pressure leads to a decrease in both the superconducting transition temperature T_c and the superconducting energy gap Δ [1–3,8–11]. At first glance, it is expected that these two quantities would change proportionally to each other. This expectation is dictated, in particular, by the universal relation established within Bardeen-Cooper-Schrieffer (BCS) theory [12,13]:

$$\alpha_{BCS} = \frac{\Delta}{k_B T_c} = \frac{\pi}{e^{\gamma_E}} \simeq 1.764, \tag{1}$$

where γ_E and k_B are the Euler and Boltzmann constants, respectively. Experimentally, however, it was found that Δ decreases faster than T_c, suggesting that $\alpha = \Delta/k_B T_c$ is, in fact, pressure dependent [8,9,14,15].

Note, that in superconductor physics $\alpha = \Delta/k_B T_c$ has a special meaning and is offen called the coupling strength. By comparing αs with the universal BCS value α_{BCS}, the superconductors are divided into strong-coupling ($\alpha \gg 1.764$), intermediate-coupling ($\alpha \gtrsim 1.764$) and weak-coupling ($\alpha \simeq 1.764$) classes. The BCS theory implies that in a case of a single, uniform (in both real and momentum space) order parameter, $\alpha_{BCS} \simeq 1.764$ sets the lower bound for possible coupling strength values. In other words, weaker coupling, *i.e.*, $\alpha < \alpha_{BCS}$ becomes physically impossible.

Regarding the above-mentioned faster decrease of Δ compared to T_c, two important consequences are expected to follow: (i) Pressure reduces the coupling strength α and moves the superconductor into the weak-coupling direction. (ii) As α approaches the weak-coupling BCS value $\alpha_{BCS} = 1.764$, the coupling strength should saturate and remain unchanged with further increases in pressure. The first statement was indeed confirmed in tunneling studies of various conventional superconductors, suggesting the universality of the trend. Experiments reveal that moderate pressures (up to ∼2.0 GPa) lead to substantial decrease in α in various single-element and binary superconducting materials [8,9,14,15]. The second trend, namely the saturation of α as it approaches α_{BCS}, has not been experimentally confirmed so far. On the contrary, measurements of the thermodynamic critical field B_c in

*Contact author: rustem.khasanov@psi.ch

†Contact author: giovanni.ummarino@polito.it

Published by the American Physical Society under the terms of the Creative Commons Attribution 4.0 International license. Further distribution of this work must maintain attribution to the author(s) and the published article's title, journal citation, and DOI.

elemental aluminum reveal that α may decrease below the $\alpha_{\rm BCS}$ level due to enhanced anisotropy of the superconducting energy gap [16].

From the theoretical side, Leavens and Carbotte, Ref. [17], have shown that the effect of pressure on the energy gap in conventional phonon-mediated superconductors is expected to be twofold. First, pressure decreases the mean gap value much more significantly than T_c due to the effect of phonon hardening. Second, pressure is expected to increase the gap anisotropy, *i.e.*, the ratio between the largest and smallest energy gap values. This suggests that in studies of the pressure effect on coupling strength α, both of the aforementioned contributions need to be considered.

In this paper, we studied the effect of pressure on the superconducting energy gap in elemental indium (In) and tin (Sn). The average values of the superconducting energy gap ($\langle\Delta\rangle$) were determined from measurements of the temperature evolution of the thermodynamic critical field B_c using the muon-spin rotation/relaxation technique. The analysis of the experimental data within the phenomenological α-model of Padamsee *et al.* [18,19] suggests that an increase in pressure from $p = 0.0$ to $\simeq 3.0$ GPa leads to a decrease in $\alpha = \langle\Delta\rangle/k_BT_c$ from 1.89 to 1.78 for indium and from 1.83 to 1.77 for tin, respectively. A simple model based on Eliashberg theory allows us to distinguish between the enhancement of a gap anisotropy and the phonon hardening effects.

II. EXPERIMENTAL DETAILS

Sn and In samples were prepared from commercially available solid pieces ($\simeq 3-4$ mm in size). The clean metals were obtained from Alfa Aesar (tin, 99.999% purity) and ChemPur (indium, 99.9999% purity). Pieces of soft In and Sn metal were placed inside the 5 mm in diameter ($d = 5$ mm) pressure cell channel and pressed with a force of $\sim 1-1.5$ ton. Following this procedure, the metal fills the pressure cell channel and forms cylindrically shaped samples. The amount of material was chosen to achieve the compressed sample height approximately 15 mm ($h \simeq 15$ mm). No pressure medium was used. The pressure cell consisted of three cylinders (three-wall pressure cell), where under ambient conditions each inner cylinder remains precompressed by the outer one. The construction and the characteristics of the three-wall pressure cell are described in Ref. [20].

The muon-spin rotation/relaxation (μSR) under pressure experiments were performed at the μE1 beamline using the General Purpose Decay (GPD) spectrometer, Paul Scherrer Institute, PSI Villigen, Switzerland [21,22]. The ^{4}He cryostat equipped with the ^{3}He inset was used. The external magnetic field $B_{\rm ap}$ was applied perpendicular to the initial muon-spin direction, corresponding to the transverse-field (TF-μSR) geometry. The experiments were conducted in the temperature range of 0.25 to 4.0 K and in the field range of 0.5 to 40 mT.

The TF-μSR measurements were performed in the intermediate state, *i.e.*, when the type-I superconducting sample is separated on the normal state (NS) and the superconducting (SC) [*i.e.*, Meissner domains, see *e.g.*, Refs. [23–31] and schematic in Fig. 1(a)]. The magnetic field $B_{\rm ap}$ was applied perpendicular to the cylindrical axis of the sample. In this geometry the sample's demagnetization factor is estimated to be $n = (2 + d/\sqrt{2}h)^{-1} \simeq 0.45$ [32], and the intermediate state is expected to form for applied fields in the range $B_c < B_{\rm ap} \lesssim 0.55 \cdot B_c$. The modified $B-T$ scan measuring scheme, as discussed in Refs. [24,26], was used. At each particular temperature, the measured points were reached by first increasing $B_{\rm ap}$ above B_c ($B_{\rm ap} \simeq 35$ mT) and then decreasing it back to the measurement field. The $B-T$ points were taken along the $\simeq 0.7 \cdot B_c(T)$, and $0.8 \cdot B_c(T)$ lines. The TF-μSR data analysis procedure and the way of obtaining B_c from TF-μSR data are described in Appendix A.

III. EXPERIMENTAL DATA AND DISCUSSIONS

A. Pressure dependences of the thermodynamic critical field B_c in In and Sn

The magnetic field distribution in type-I superconductor in the intermediate state, which is probed directly by means of TF-μSR, consists of two peaks corresponding to the response of the domains remaining in the superconducting Meissner state ($B = 0$) and in the normal state ($B = B_c > B_{\rm ap}$) [see the schematic representation at Fig. 1(a) and the raw μSR data at Fig. 4 in Appendix A]. Consequently, in TF-μSR experiments the value of B_c is directly and very precisely determined by measuring the position of $B > B_{\rm ap}$ peak [23–26,33–38].

The Fourier transforms of TF-μSR data for superconducting Sn sample measured at $p \simeq 1.6$ Gpa are shown in Fig. 1(b). The figure represents part of the experimental data accumulated at $B-T$ scan with $B_{\rm ap} \simeq 0.7 \cdot B_c(T)$. Note that in addition to $B = 0$ and $B = B_c$ peaks corresponding to the response of the sample, the background peak caused by muons stopped in the pressure cell walls [denoted as PC background in Fig. 1(b)] is also seen. The mean value of the background field is equal to $B_{\rm ap}$, while the broadening of the background signal is caused by the influence of the sample's stray field on the pressure cell walls [39].

The temperature dependences of the thermodynamic critical field B_c at pressures ranging from $p = 0.0$ to $\simeq 3$ GPa are presented in Figs. 1(c) and 1(d) for the In and Sn samples, respectively. Deviations of the B_c *vs.* T curves from the parabolic function $D(T/T_c) = B_c(T/T_c)/B_c(0) - [1-(T/T_c)^2]$, where $B_c(0)$ is the zero-temperature value of the thermodynamic critical field, are shown in Figs. 1(e) and 1(f). The analysis of $B_c(T,p)$ dependences was performed within the framework of the phenomenological α-model of Padamsee *et al.* [18,19], allowing the $B_c(T)$ dependences to be analyzed with only three independent parameters: T_c, $B_c(0)$, and Δ (see Appendix B for details). Fits of the α-model to the $B_c(T)$ data are shown by solid lines in Figs. 1(c)–1(f).

Figure 2 shows dependences of T_c, $B_c(0)$, and the average value of the superconducting gap ($\langle\Delta\rangle$) on the applied pressure. Asterisks correspond to the values obtained from fits of $B_c(T)$ curves for indium and tin reported by Finnemore and Mapother in Ref. [40]. It should be noted that our experiments were performed on nonoriented metallic samples, so the value of the superconducting gap corresponds to a mean (*i.e.*, averaged) $\langle\Delta\rangle$ value. Figure 2 suggests, that for both In and Sn samples, all three thermodynamic quantities decrease nearly linearly with increasing pressure. The solid lines represent linear fits, with the parameters summarized in Table I.

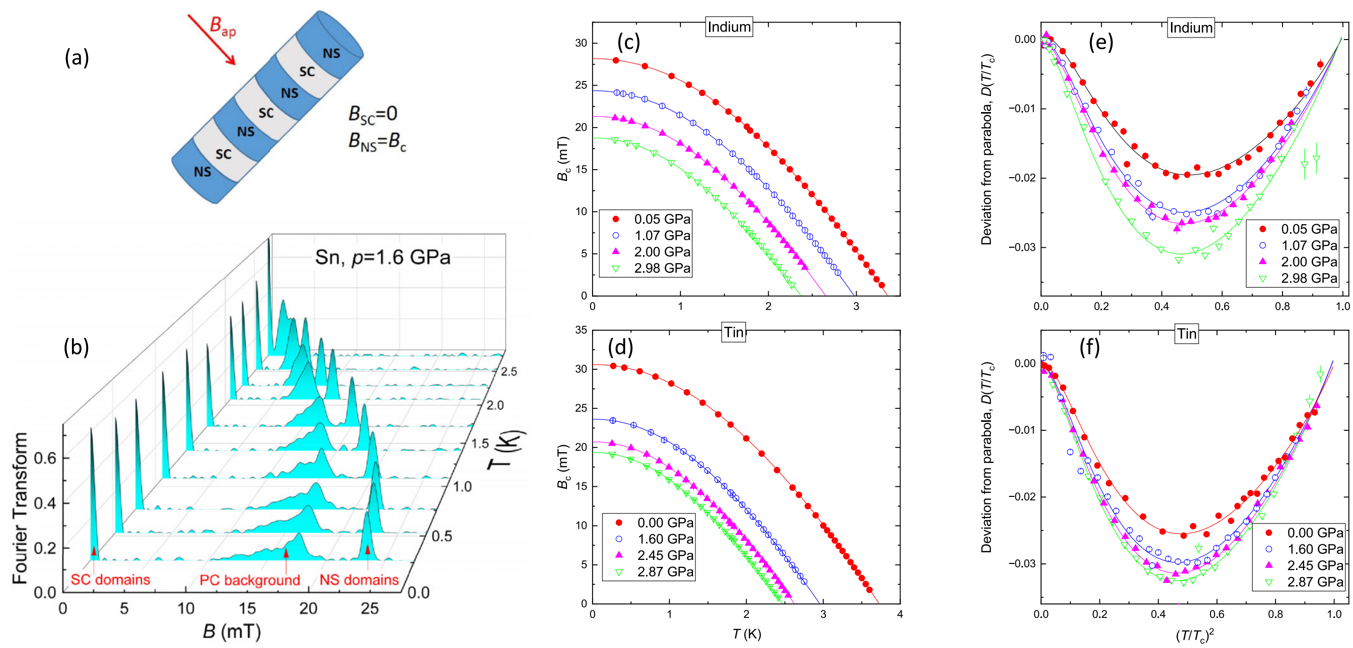

FIG. 1. (a) The schematic representation of separation of a type-I cylindrical sample into the normal state (NS) and the superconducting (SC) domains. The magnetic field in NS domains is equal to the thermodynamic critical field, $B_{NS} = B_c$. The field in SC domains is equal to zero, $B_{SC} = 0$. (b) Fourier transforms of TF-μSR data for the tin sample measured at $p = 1.60$ GPa. Peaks at $B = 0$, $B = B_c$, and $B \simeq B_{ap}$ correspond to the contributions of the superconducting domains, normal state domains, and the background caused by the pressure cell, respectively. (c) Temperature dependences of the thermodynamic critical field B_c in elemental indium measured at pressures $p = 0.05$, 1.07, 2.09, and 2.98 GPa. (d) $B_c(T)$ dependences in elemental tin measured at $p = 0.0$, 1.60, 2.45, and 2.87 GPa. (e) Deviation functions $D(T/T_c) = B_c(T/T_c)/B_c(0) - [1 - (T/T_c)^2]$ as obtained for the indium sample. (f) $D(T/T_c)$ dependences for the tin sample. The solid lines in (c)-(f) are fits of phenomenological α-model to the $B_c(T)$ data (see Appendix B for details).

From the data presented in Fig. 2 and Table I, the following three important points emerge:

(i) The zero-pressure values of the superconducting transition temperature T_c, the thermodynamic critical field $B_c(0)$, and the averaged superconducting energy gap $\langle\Delta\rangle$, as well as the pressure slopes of T_c and $\langle\Delta\rangle$, are in a good agreement with the literature data [1–3,8,9,14,15,27,40,41].

(ii) With increasing pressure, the superconducting energy gap $\langle\Delta\rangle$ decreases faster than the transition temperature T_c, in agreement with the results reported in the literature [9,14,15].

(iii) The relative pressure shifts of the thermodynamic critical field $B_c(0)$ and the superconducting energy gap $\langle\Delta\rangle$ are the same within experimental uncertainties. This could be due to the fact that $B_c(0)$ is the measure of the energy, which has to be supplied to the material to destroy superconductivity. This implies that both $B_c(0)$ and $\langle\Delta\rangle$ are subject to similar energy scales in conventional phonon-mediated superconductors.

B. Pressure evolution of the coupling strengths $\alpha = \langle\Delta\rangle/k_BT_c$

Figure 3 shows the dependences of $\alpha = \langle\Delta\rangle/k_BT_c$ on pressure. In both In and Sn samples, α decreases with increasing pressure. In the indium sample, α changes from 1.89(1) at ambient pressure to 1.78(1) at $p \simeq 3.0$ GPa [Fig. 3(a)], while in the tin sample it decreases from 1.83(1) to 1.77(1) as pressure increases from 0 to $\simeq 2.9$ GPa [Fig. 3(b)]. Following the definition of $\alpha = \Delta/k_BT_c$ as the coupling strength (see above), this implies that pressure lowers the coupling strength and moves both In and Sn superconductors from the intermediate-coupling to the weak-coupling regime. Note that the effect of decreased coupling is also seen in $D(T/T_c)$ data [Figs. 1(e) and 1(f)] implying that pressure increases the deviation of $B_c(T)$ curves from parabolic behavior.

The linear fits of $\alpha(p)$ presented in Fig. 3 yield $\alpha(p) = 1.892(5) - 0.037(2) \cdot p$ for In and $\alpha(p) = 1.833(5) - 0.024(4) \cdot p$ for Sn superconducting sample,

TABLE I. Pressure dependences of thermodynamic parameters for In and Sn samples. $T_c(p=0)$ is the superconducting transition temperature at $p = 0$, $B_c(0, p=0)$ is the zero-temperature zero-field value of the thermodynamic critical field, and $\langle\Delta(p=0)\rangle$ is the average zero-pressure value of the superconducting energy gap.

Sample	$T_c(p=0)$ (K)	dT_c/dp (K/GPa)	$d\ln T_c/dp$ (1/GPa)	$B_c(0, p=0)$ (mT)	$dB_c(0)/dp$ (mT/Gpa)	$d\ln B_c(0)/dp$ (1/GPa)	$\langle\Delta(p=0)\rangle$ (mev)	$d\langle\Delta\rangle/dp$ (meV/GPa)	$d\ln\langle\Delta\rangle/dp$ (1/GPa)
Indium	3.39(2)	−0.346(1)	−0.102(1)	28.15(5)	−3.25(6)	−0.115(2)	0.550(4)	−0.0643(5)	−0.117(2)
Tin	3.71(2)	−0.440(1)	−0.119(1)	30.45(6)	−3.94(5)	−0.129(2)	0.586(6)	−0.0748(5)	−0.126(2)

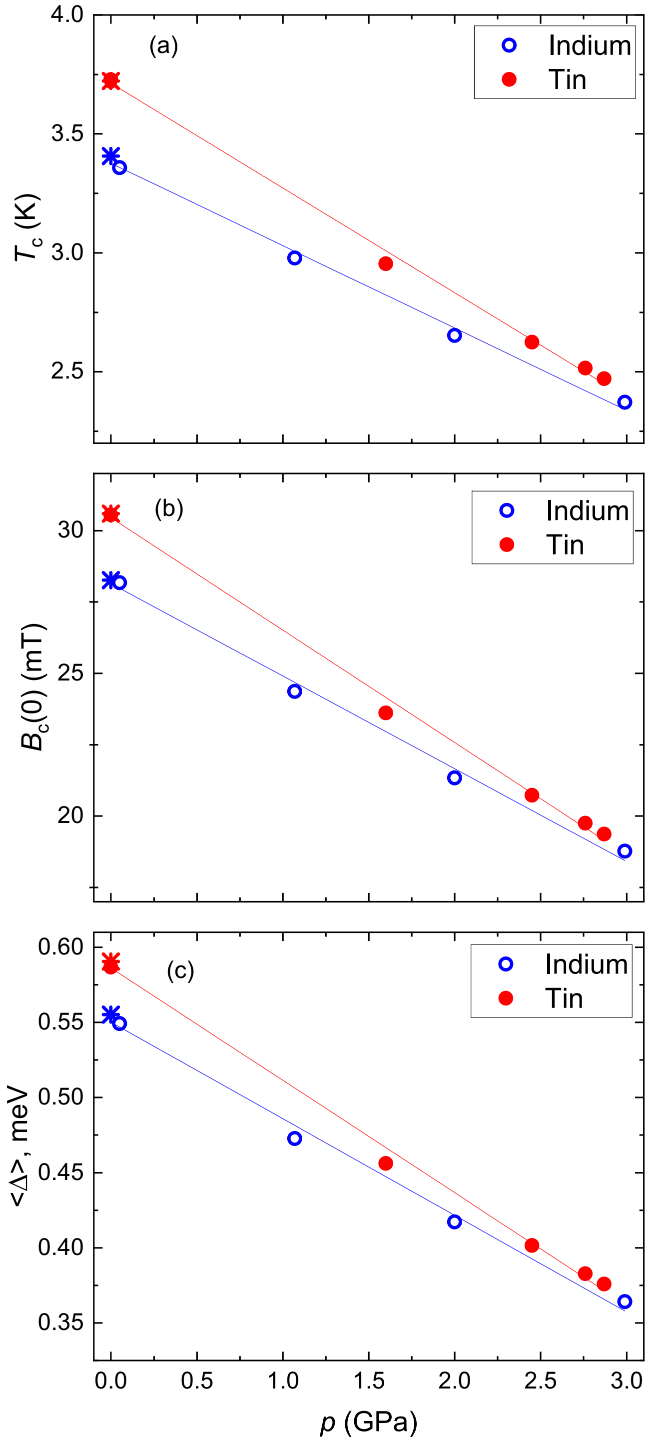

FIG. 2. Pressure dependence of (a) the superconducting transition temperatures T_c; (b) the zero-temperature values of the thermodynamic critical fields $B_c(0)$; and (c) the mean values of the superconducting energy gaps $\langle\Delta\rangle$ for In and Sn samples. These quantities are obtained from the analysis of $B_c(T, p)$ data within the framework of the phenomenological α-model of Padamsee *et al.* [18,19]. The circles correspond to the data obtained in the present study. The asterisks represent parameters obtained from the analysis of the data of Finnemore and Mapother [40]. The solid lines are linear fits.

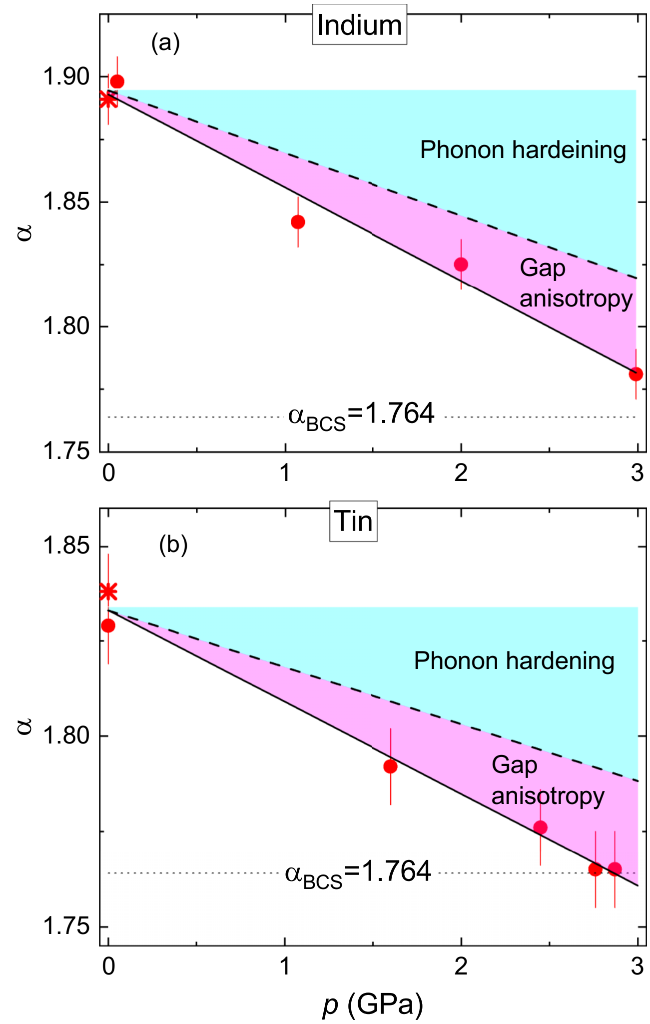

FIG. 3. (a) Dependence of the coupling strength $\alpha = \langle\Delta\rangle/k_B T_c$ on applied pressure p for the indium sample. Red circles correspond to the experimental data. The phonon hardening and anisotropic contributions are shown in light blue and pink, respectively. The solid and dashed lines are linear fits with $\alpha(p) = 1.892(5) - 0.037(2) \cdot p$ and $\alpha(p) = 1.894(2) - 0.025(1) \cdot p$, respectively (see text for further details). (b) The same as in (a), but for the tin sample. The solid and dashed lines correspond to linear fits with $\alpha(p) = 1.833(5) - 0.024(4) \cdot p$ and $\alpha(p) = 1.833(3) - 0.015(1) \cdot p$, respectively (see text for further details). The dotted lines in (a) and (b) represent the universal BCS value $\alpha_{BCS} = 1.764$. The asterisks are parameters obtained from the analysis of the data of Finnemore and Mapother [40].

respectively. Comparison with the universal weak-coupling BCS value $\alpha_{BCS} = 1.764$, which sets the lower limit for the possible coupling strengths in phonon-mediated superconductors with an isotropic energy gap, implies that $\alpha(p)$ data would approach the α_{BCS} value at $p \simeq 3.55$ GPa for In and $p \simeq 2.89$ GPa for Sn, respectively. If we were able to reach pressures higher than these limiting values, it might be possible to test the hypothesis that α values smaller than α_{BCS} cannot be achieved. It is interesting to note that the last two points measured at pressures $p = 2.45$ and 2.87 GPa in the tin sample result in similar $\alpha = 1.765(10)$ values, which may indicate the saturation of α precisely at the weak-coupling BCS value $\alpha_{\rm BCS} = 1.764$. However, more measurements at higher pressures are needed to confirm or refute this observation.

Leavens and Carbotte [17], have shown that the effect of pressure on α in conventional phonon-mediated superconductors consist of two components. The first contribution arises from phonon hardening effects, while the second is determined by pressure-induced changes in the gap anisotropy. In Appendix C we describe a simple model that allows us to determine the pressure dependence of the phonon contribution to the coupling strength. The resulting phonon hardening and anisotropic contributions are presented in Fig. 3 in light blue and pink colors, respectively. Clearly, only part of the pressure effect on $\langle\Delta\rangle/k_{\rm B}T_{\rm c}$ can be attributed to the phonon term. Nearly 40% of the effect is likely caused by the pressure-induced increase in the anisotropy of the superconducting energy gap. It is worth noting that the enhancement of gap anisotropy due to applied pressure was recently reported for elemental aluminum [16]. Considering that our experiments were performed on non-oriented samples, the thermodynamic quantities reported here, namely $B_{\rm c}$ and Δ, correspond to averaged values. This does not allow us to speculate on the angular dependence of the superconducting energy gap, nor to obtain the absolute value of the gap anisotropy.

IV. CONCLUSIONS

To conclude, the pressure dependence of the thermodynamic critical field $B_{\rm c}$ in elemental superconductors indium (In) and tin (Sn) was studied using the muon-spin rotation/relaxation technique. With the pressure increase from 0.0 to $\simeq 3.0$ GPa, the coupling strength $\alpha = \langle\Delta\rangle/k_{\rm B}T_{\rm c}$ decreases: from 1.89 to 1.78 for indium and from 1.83 to 1.77 for tin, respectively. Linear fits suggest that the coupling strength approaches the limiting weak-coupling BCS value $\alpha_{\rm BCS} = 1.764$ at $p \simeq 3.55$ GPa for In and $\simeq 2.89$ GPa for Sn. This implies that pressure lowers the coupling strength and moves both In and Sn superconductors from the intermediate-coupling to the weak-coupling regime. The analysis of $\alpha(p)$ data within the framework of the Eliashberg theory reveals that only part of the pressure effect might be attributed to the hardening of the phonon spectra, which is reflected in a decrease of the electron-phonon coupling constant. Nearly 40% of the effect is caused by increased anisotropy of the superconducting energy gap.

ACKNOWLEDGMENTS

This work was performed at the Swiss Muon Source (SμS), Paul Scherrer Institute (PSI, Switzerland). R.K. acknowledges helpful discussions with R. Gupta and D. Das.

APPENDIX A: TF-μSR DATA ANALYSIS PROCEDURE

The experimental TF-μSR data were analyzed by separating the signal into the sample (s) and the pressure cell (pc) contributions:

$$A_0P(t) = A_{\rm s}P_{\rm s}(t) + A_{\rm pc}P_{\rm pc}(t). \quad \text{(A1)}$$

Here, A_0 represents the initial asymmetry of the muon-spin ensemble, while $A_{\rm s}$ ($A_{\rm pc}$) and $P_{\rm s}(t)$ [$P_{\rm pc}(t)$] denote the asymmetry and the time evolution of the muon-spin polarization for the sample (pressure cell), respectively.

The sample part was described by considering the contributions from the normal state (NS) and the superconducting (SC) domains:

$$P_{\rm s}(t) = f_{\rm NS}\, e^{-\lambda_{\rm NS}t}\, \cos(\gamma_\mu B_{\rm NS}t + \phi) + f_{\rm SC}\left[\tfrac{1}{3} + \tfrac{2}{3}\left(1 - \sigma_{\rm GKT}^2 t^2\right)e^{-\sigma_{\rm GKT}^2t^2/2}\right]. \quad \text{(A2)}$$

The first term on the right-hand side of the equation corresponds to the sample's normal state response: $f_{\rm NS}$ is the volume fraction of normal state domains ($f_{\rm NS} = 1$ for $T \geqslant T_{\rm c}$), $\lambda_{\rm NS}$ is the exponential relaxation rate, and $B_{\rm NS}$ is the internal field [$B_{\rm NS} = B_{\rm c}$ for $T < T_{\rm c}(B_{\rm ap})$ and $B_{\rm NS} = B_{\rm ap}$ for $T \geqslant T_{\rm c}(B_{\rm ap})$, respectively]. The second term describes the contribution of the superconducting part of the sample remaining in the Meissner state ($B_{\rm SC} = 0$). $f_{\rm SC} = 1 - f_{\rm NS}$ is the superconducting volume fraction. The term is approximated by the Gaussian Kubo-Toyabe (GKT) function with the relaxation rate $\sigma_{\rm GKT}$, which is generally used to describe the nuclear magnetic moment contribution in zero-field experiments (see, *e.g.,* Refs. [42,43] and references therein). The pressure cell contribution was described by

$$P_{\rm pc}(t) = e^{-\lambda_{\rm pc}t}\, \cos(\gamma_\mu B_{\rm ap}t + \phi). \quad \text{(A3)}$$

Here, $\lambda_{\rm pc}$ is the exponential relaxation rate caused by the pressure cell material.

Figure 4(a) shows the TF-μSR time spectra collected on the tin sample at $T = 0.26$ K, $p = 2.87$ GPa, and $B_{\rm ap} = 14.0$ and 16.0 mT. The solid lines correspond to the fit of Eq. (A1) to the experimental data. The Fourier transformations of TF-μSR time spectra presented in panel (a) are shown in Fig. 4(b). The peaks at $B = 0$ and $B = B_{\rm c}$ denote the response of the Meissner (superconducting) and the normal state domains, respectively. Peaks at $B = B_{\rm ap}$ represent the pressure cell contribution.

APPENDIX B: $\alpha-$ MODEL IN ANALYSING $B_{\rm c}(T)$ DATA

The α-model assumes that the normalized superconducting energy gap is described as:

$$\delta(t) = \frac{\Delta(t)}{\Delta} = \frac{\Delta_{\rm BCS}(t)}{\Delta_{\rm BCS}}. \quad \text{(B1)}$$

Here, Δ is the zero-temperature value of the gap, and $t = T/T_{\rm c}$ is the reduced temperature. The function $\delta(t)$ is the same as in BCS theory [44], and it is calculated using the BCS value $\alpha_{\rm BCS} = 1.764$. On the other hand, to calculate the temperature evolution of the electronic free energy, entropy, heat capacity and thermodynamic critical field, the α-model assumes $\alpha = \Delta/k_{\rm B}T_{\rm c}$ is an adjustable parameter.

The temperature evolution of $B_{\rm c}$ can be determined from the difference between the normal state and the

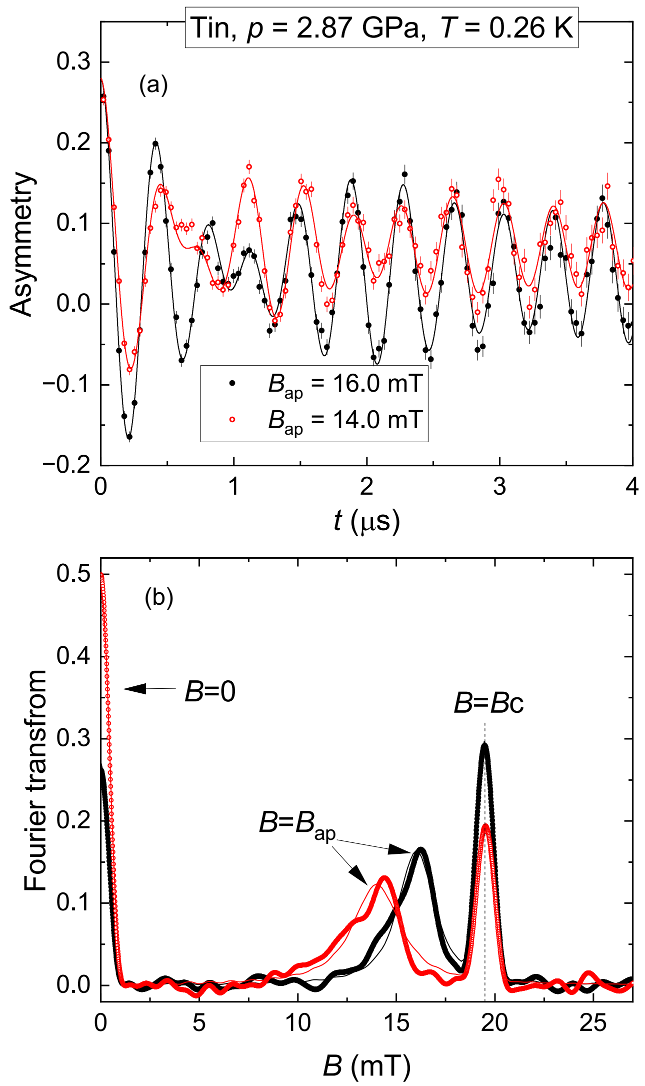

FIG. 4. (a) TF-μSR time spectra for a tin sample taken at $T \simeq 0.26$ K, $p = 2.87$ GPa, and $B_{ex} = 14.0$ (red symbols) and 16.0 mT (black symbols), respectively. The solid lines are fits of Eq. (A1) [with the sample and pressure cell contributions described by Eqs. (A2) and (A3)] to the experimental data. (b) Fourier transforms of TF-μSR time-spectra presented in (a). Arrows indicate the positions of the zero field in the superconducting domains ($B_{SC} = 0$), the thermodynamic critical field in the normal state domains ($B_{NS} = B_c$) and the applied field (B_{ap}) in the pressure cell.

superconducting state entropies $S_{NS} - S_{SC}$ via [18,19]:

$$\frac{B_c^2}{8\pi} = T_c \int_t^1 [S_{NS}(t') - S_{SC}(t')]dt' \tag{B2}$$

with

$$\frac{S_{NS}(t)}{\gamma_e T_c} = t$$

and

$$\frac{S_{SC}(t)}{\gamma_e T_c} = \frac{6\alpha^2}{\pi^2 t} \int_0^\infty f(\alpha, E, t)\left(E + \frac{\varepsilon^2}{E}\right)d\varepsilon.$$

TABLE II. The initial parameters used for solving the Eliashberg equations ($p = 0$). λ is the electron-phonon coupling constant, $\mu^*(\omega_c)$ is the Coulomb pseudopotential, Ω_0 $T_c(p = 0)$ is a typical phon frequency, Ω_{log} is the logarithmic cutoff frequency, ω_c is a cutoff energy, ω_{max} is a maximum quasiparticle energy, and γ_G is the Grüneisen parameter.

	λ	$\mu^*(\omega_c)$	Ω_0 (meV)	Ω_{log} (meV)	ω_c (meV)	ω_{max} (meV)	γ_G
In	0.81	0.095149	5.10	5.83	48	50	2.55
Sn	0.72	0.137460	9.00	9.90	57	60	2.57

Here, $f(\alpha, E, t) = [\exp(\alpha E/t) + 1]^{-1}$ is the Fermi function, $E = E(\varepsilon, \delta(t)) = [\varepsilon^2 + \delta(t)^2]^{0.5}$, and γ_e is the normal state electronic specific heat coefficient. The temperature dependence of the normalized gap, Eq. (B1), is described as $\delta(t) = \tanh\{1.82[1.018(1/t - 1)]^{0.51}\}$ [45], which is a simplified version of Mühlschlegel's BCS approximation reported in Ref. [44].

APPENDIX C: CALCULATIONS OF THE PHONON-HARDENING CONTRIBUTIONS ON THE COUPLING CONSTANT $\langle\Delta\rangle/k_B T_c$

The calculations were performed within the s-wave Eliashberg approach by solving two coupled equations for the gap $\Delta(i\omega_n)$ and the renormalization functions $Z(i\omega_n)$ with ω_n representing Matsubara frequencies. The imaginary-axis equations, within the validity range of the Migdal theorem [46], read [41,47]:

$$\omega_n Z(i\omega_n) = \omega_n + \pi T \sum_m \Lambda(i\omega_n, i\omega_m) N^Z(i\omega_m) + [\Gamma^N + \Gamma^M] N^Z(i\omega_n) \tag{C1}$$

and

$$Z(i\omega_n)\Delta(i\omega_n) = \pi T \sum_m [\Lambda(i\omega_n, i\omega_m) - \mu^*(\omega_c) \times \Theta(\omega_c - |\omega_m|)] N^\Delta(i\omega_m) + [\Gamma^N - \Gamma^M] N^\Delta(i\omega_n). \tag{C2}$$

Here,

$$\Lambda(i\omega_n, i\omega_m) = 2\int_0^{+\infty} d\Omega \Omega \alpha^2 F(\Omega)/[(\omega_n - \omega_m)^2 + \Omega^2],$$

$$N^\Delta(i\omega_m) = \Delta(i\omega_m)/\sqrt{\omega_m^2 + \Delta^2(i\omega_m)},$$

and

$$N^Z(i\omega_m) = \omega_m/\sqrt{\omega_m^2 + \Delta^2(i\omega_m)}.$$

The parameters Γ^N and Γ^M represent the scattering rates from nonmagnetic and magnetic impurities, respectively; Θ is the Heaviside function; ω_c is a cutoff energy; $\mu^*(\omega_c)$ is the Coulomb pseudopotential, and $\alpha^2 F(\Omega)$ is the electron-phonon spectral function. The electron-phonon coupling constant is

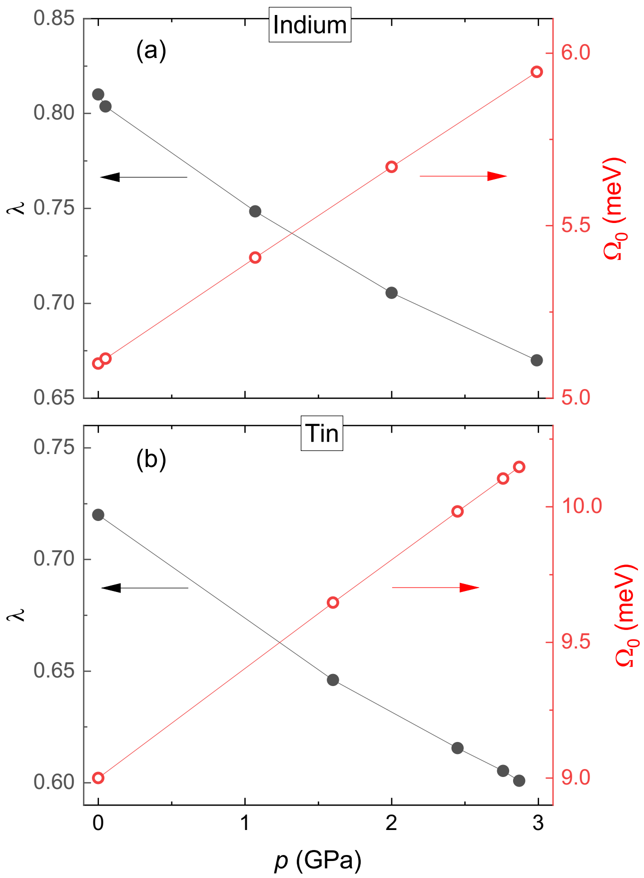

FIG. 5. (a) Pressure dependences of the coupling constant λ (closed circles) and a typical phonon energy Ω_0 (open circles) calculated within the Eliashberg approach for superconducting indium. (b) The same as in (a) but for superconducting tin.

defined as

$$\lambda = 2\int_0^{+\infty} d\Omega \frac{\alpha^2F(\Omega)}{\Omega}.$$

In general, the solution of the Eliashberg equations requires a number of input parameters. One has to introduce the electron-phonon spectral function $\alpha^2F(\Omega)$, the Coulomb pseudopotential $\mu^*(\omega_c)$, the nonmagnetic $\Gamma^{\rm N}$ and magnetic $\Gamma^{\rm M}$ impurity-scattering rates. However, some of these parameters can be extracted from experiments, and some can be fixed by suitable approximations. In particular, one may assume $\Gamma^{\rm N}=0$, since for an $s-$wave order parameter the nonmagnetic impurity scattering rate has no influence on functions $\Delta(i\omega_{\rm n})$ and $Z(i\omega_{\rm n})$. Moreover we put $\Gamma^{\rm M}=0$ because in the studied materials, high purity Sn and In samples, the magnetic impurities are absent. The electron-phonon spectral functions $\alpha^2F(\Omega)$s, the coupling constants λs, the cut-off energy $\omega_{\rm c}$ and the maximum quasiparticle energy $\omega_{\rm max}$ were obtained from Ref. [41].

To calculate the effect of pressure on $\alpha=\langle\Delta\rangle/k_BT_c$, the following minimal model was developed. The electron-phonon spectral function was assumed to have a Dirac delta function shape: $\alpha^2F(\Omega)=0.5\lambda\Omega_0\delta(\Omega-\Omega_0)$, where $\Omega_0(p=0)$ is a typical phonon energy, and $\lambda(p=0)$ is the experimental value of the electron-phonon spectral function at $p=0$ [41]. The use of such an approximation, in place of exact electron-phonon spectral function, allows for a simple calculations of the effect of pressure on the phonon spectrum. $\lambda(p=0)$ is an experimental value, so the values of $\Omega_0(p=0)$ and $\mu^*(\omega_c)$ were fixed to match the exact experimental $T_{\rm c}$ and $\langle\Delta\rangle$ values. The values of $\Omega_0(p=0)$ were found to be close to the representative energy $\Omega_{\rm log}=2\int\frac{\alpha^2F(\Omega,p=0)}{\Omega}\ln\Omega d\Omega$ of the phonon spectra [41]. The initial input parameters of the Eliashberg equations are summarized in Table II.

The pressure dependence of a typical phonon energy $\Omega_0(p)$ was calculated by using the relation [48]:

$$\frac{\Omega_0(p)}{\Omega_0(p=0)}=\frac{V(p)}{V(p=0)}^{-\gamma_{\rm G}}. \tag{C3}$$

Here $\gamma_{\rm G}$ is the Grüneisen parameter. The values of the Grüneisen parameter for In and Sn at $p=0$, as reported in Ref. [49], are shown in Table II.

The $V(p)/V(p=0)$ dependences were obtained from band calculations [50,51] and approximated by using a third-order polynomials as

$$\frac{V(p)}{V(p=0)}=1-2.224\cdot10^{-2}\ p+1.01\cdot10^{-3}\ p^2 \\ -3.43892\cdot10^{-5}\ p^3$$

and

$$\frac{V(p)}{V(p=0)}=1-1.767\cdot10^{-2}\ p+6.63325\cdot10^{-4}\ p^2 \\ -1.50771\cdot10^{-5}\ p^3$$

for In and Sn, respectively.

With $\Omega_0(p)$ calculated by means of Eq. (C3), one gets $\lambda(p)$ by solving the Eliashberg equations under the condition that the theoretically obtained transition temperature values match the experimental $T_{\rm c}(p)$ dependences as presented in Fig. 2(a). The such obtained pressure evolutions of λ and Ω_0 are shown in Fig. 5. With all the variables known [$\lambda(p)$, $\Omega_0(p)$, and $\mu^*(\omega_c)$], the gap $\Delta(i\omega_n,T)$ was calculated by solving the Eliashberg equations on the imaginary axis at low temperatures ($T=T_c/12$). Subsequently, using Padé approximants method [41], $\Delta(p)$ and the coupling constant $\Delta(p)/k_{\rm B}T_{\rm c}$ were calculated. Finally, the phonon-hardening contributions on the coupling constant α were obtained as $\alpha(p)=1.894(2)-0.025(1)\cdot p$ for In and $\alpha(p)=1.833(3)-0.015(1)\cdot p$ for Sn superconducting samples, respectively.

[1] B. Lorenz and C. Chu, High pressure effects on superconductivity, in *Frontiers in Superconducting Materials*, edited by A. V. Narlikar (Springer, Berlin, 2005).

[2] J. S. Schilling, High-pressure effects, in *Handbook of High-Temperature Superconductivity*, edited by J. R. Schrieffer and J. S. Brooks (Springer, New York, 2007).

[3] J. S. Schilling and J. J. Hamlin, Recent studies in superconductivity at extreme pressures, J. Phys.: Conf. Ser. **121**, 052006 (2008).
[4] H. Sun, M. Huo, X. Hu, J. Li, Z. Liu, Y. Han, L. Tang, Z. Mao, P. Yang, B. Wang, J. Cheng, D.-X. Yao, G.-M. Zhang, and M. Wang, Signatures of superconductivity near 80 K in a nickelate under high pressure, Nature (London) **621**, 493 (2023).
[5] M. Somayazulu, M. Ahart, A. K. Mishra, Z. M. Geballe, M. Baldini, Y. Meng, V. V. Struzhkin, and R. J. Hemley, Evidence for superconductivity above 260 K in lanthanum superhydride at megabar pressures, Phys. Rev. Lett. **122**, 027001 (2019).
[6] A. P. Drozdov, P. P. Kong, V. S. Minkov, S. P. Besedin, M. A. Kuzovnikov, S. Mozaffari, L. Balicas, F. Balakirev, D. Graf, V. B. Prakapenka, E. Greenberg, D. A. Knyazev, M. Tkacz, and M. I. Eremets, Superconductivity at 250 K in lanthanum hydride under high pressures, Nature (London) **569**, 528 (2019).
[7] D. V. Semenok, I. A. Troyan, Di Zhou, A. V. Sadakov, K. S. Pervakov, O. A. Sobolevskiy, A. G. Ivanova, Michele Galasso, F. G. Alabarse, W. Chen, C. Xi, T. Helm, S. Luther, V. M. Pudalov, and V. V. Struzhkin, Ternary superhydrides under pressure of Anderson's theorem: Near-record superconductivity in (La, Sc)H_{12}, arXiv:2408.07477.
[8] J. P. Franck and W. J. Keeler, Pressure dependence of the energy gap of superconducting Pb, Phys. Rev. Lett. **20**, 379 (1968).
[9] V. M. Svistunov, M. A. Belogolovskii, and O. I. Chernyak, Tunnel investigations of metals at high pressures, Sov. Phys. Usp. **30**, 1 (1987).
[10] J. Zhu, Z.-X. Yang, X.-Y. Hou, T. Guan, Q.-T. Zhang, Y.-Q. Li, X.-F. Han, J. Zhang, C.-H. Li, L. Shan, G.-F. Chen, and C. Ren, Tunneling spectroscopy of Al/AlO_x/Pb subjected to hydrostatic pressure, Appl. Phys. Lett. **106**, 202601 (2015).
[11] F. Du, F. F. Balakirev, V. S. Minkov, G. A. Smith, B. Maiorov, P. P. Kong, A. P. Drozdov, and M. I. Eremets, Tunneling spectroscopy at megabar pressures: Determination of the superconducting gap in sulfur, Phys. Rev. Lett. **133**, 036002 (2024).
[12] J. Bardeen, L. N. Cooper, and J. R. Schrieffer, Microscopic theory of superconductivity, Phys. Rev. **106**, 162 (1957).
[13] M. Tinkham, *Introduction to Superconductivity* (Krieger, Malabar, FL, 1975).
[14] A. A. Galkin, V. M. Svistunov, A. P. Dikii, Effect of high pressure on the energy gap of indium and thallium superconducting films, Phys. Status Solidi **35**, 421 (1969).
[15] P. Nédellec and R. J. Noer, Tunneling in superconducting indium under pressure, Solid State Commun. **13**, 89 (1973).
[16] R. Khasanov and I. I. Mazin, Anomalous gap ratio in anisotropic superconductors: Aluminum under pressure, Phys. Rev. B **103**, L060502 (2021).
[17] C. R. Leavens and J. P. Carbotte, Pressure dependence of the energy gap anisotropy in aluminum, Can. J. Phys. **50**, 2568 (1972).
[18] H. Padamsee, J. E. Neighbor, and C. A. Shiffman, Quasiparticle phenomenology for thermodynamics of strong-coupling superconductors, J. Low Temp. Phys. **12**, 387 (1973).
[19] D. C. Johnston, Elaboration of the α-model derived from the BCS theory of superconductivity Supercond. Sci. Technol. **26**, 115011 (2013).
[20] R. Khasanov, R. Urquhart, M. Elender, K. Kamenev, Three-wall piston-cylinder type pressure cell for muon-spin rotation/relaxation experiments, High Press. Res. **42**, 29 (2022).
[21] R. Khasanov, Z. Guguchia, A. Maisuradze, D. Andreica, M. Elender, A. Raselli, Z. Shermadini, T. Goko, F. Knecht, E. Morenzoni, and A. Amato, High pressure research using muons at the Paul Scherrer Institute, High Press. Res. **36**, 140 (2016).
[22] R. Khasanov, Perspective on muon-spin rotation/relaxation under hydrostatic pressure, J. Appl. Phys. **132**, 190903 (2022).
[23] R. Khasanov, M. M. Radonjić, H. Luetkens, E. Morenzoni, G. Simutis, S. Schönecker, W. H. Appelt, A. Östlin, L. Chioncel, and A. Amato, Superconducting nature of the Bi-II phase of elemental bismuth, Phys. Rev. B **99**, 174506 (2019).
[24] R. Karl, F. Burri, A. Amato, M. Donegà, S. Gvasaliya, H. Luetkens, E. Morenzoni, and R. Khasanov, Muon spin rotation study of type-I superconductivity: Elemental β-Sn, Phys. Rev. B **99**, 184515 (2019).
[25] R. Khasanov, H. Luetkens, A. Amato, and E. Morenzoni, Structural phases of elemental Ga: Universal relations in conventional superconductors, Phys. Rev. B **101**, 054504 (2020).
[26] R. Khasanov, R. Gupta, D. Das, A. Amon, A. Leithe-Jasper, and E. Svanidze, Multiple-gap response of type-I noncentrosymmetric BeAu superconductor, Phys. Rev. Res. **2**, 023142 (2020).
[27] C. Poole, H. Farach, R. Creswick, and R. Prozorov, *Superconductivity*, 3rd ed. (Elseiver, Amsterdam, 2014).
[28] P. G. de Gennes, *Superconductivity of Metals and Alloys* (Benjamin, New York, 1966).
[29] C. Kittel, *Introduction to Solid State Physics,* 7th ed. (Wiley, India, 2007).
[30] R. Prozorov, Equilibrium topology of the intermediate state in type-I superconductors of different shapes, Phys. Rev. Lett. **98**, 257001 (2007).
[31] R. Prozorov, A. F. Fidler, J. R. Hoberg, and P. C. Canfield, Suprafroth in type-I superconductors, Nat. Phys. **4**, 327 (2008).
[32] R. Prozorov and V. G. Kogan, Effective demagnetizing factors of diamagnetic samples of various shapes, Phys. Rev. Appl. **10**, 014030 (2018).
[33] V. S. Egorov, G. Solt, C. Baines, D. Herlach, and U. Zimmermann, Superconducting intermediate state of white tin studied by muon-spin-rotation spectroscopy, Phys. Rev. B **64**, 024524 (2001).
[34] H. Leng, J.-C. Orain, A. Amato, Y. K. Huang, and A. de Visser, Type-I superconductivity in the Dirac semimetal $PdTe_2$ probed by μSR, Phys. Rev. B **100**, 224501 (2019).
[35] M. Gladisch, D. Herlach, H. Metz, H. Orth, G. Z. Putlitz, A. Seeger, H. Teichler, W. Wahl, and W. Wigand, Muon spin rotation in superconductors, Hyperfine Interact. **6**, 109 (1979).
[36] V. G. Grebinnik, I. I. Gurevich, V. A. Zhukov, A. I. Klimov, L. A. Levina, V. N. Maiorov, A. P. Manych, E. V. Mel'nikov, B. A. Nikol'skii, A. V. Pirogov, A. N. Ponomarev, V. S. Roganov, V. I. Selivanov, and V. A. Suetin, Investigation of superconductors by the muon technique, Zh. Eksp. Teor. Fiz. **79**, 518 (1980) [Sov. Phys. JETP **52**, 261 (1980)].
[37] J. Beare, M. Nugent, M. N. Wilson, Y. Cai, T. J. S. Munsie, A. Amon, A. Leithe-Jasper, Z. Gong, S. L. Guo, Z. Guguchia, Y. Grin, Y. J. Uemura, E. Svanidze, and G. M. Luke, μSR and magnetometry study of the type-I superconductor BeAu, Phys. Rev. B **99**, 134510 (2019).
[38] V. Kozhevnikov, A. Suter, T. Prokscha, and C. Van Haesendonck, Experimental Study of the magnetic field distribution and shape of domains near the surface of a type-I superconductor in the intermediate state, J. Supercond. Nov. Magn. **33**, 3361 (2020).

[39] A. Maisuradze, A. Shengelaya, A. Amato, E. Pomjakushina, and H. Keller, Muon spin rotation investigation of the pressure effect on the magnetic penetration depth in $YBa_2Cu_3O_x$, Phys. Rev. B **84**, 184523 (2011).

[40] D. K. Finnemore and D. E. Mapother, Superconducting Properties of Tin, Indium, and Mercury below 1° K, Phys. Rev. **140**, A507 (1965).

[41] J. P. Carbotte, Properties of boson-exchange superconductors, Rev. Mod. Phys. **62**, 1027 (1990).

[42] A. Yaouanc, and P. Dalmas de Réotier, *Muon Spin Rotation, Relaxation and Resonance: Applications to Condensed Matter* (Oxford University Press, Oxford, 2011).

[43] A. Amato and E. Morenzoni, in *Introduction to Muon Spin Spectroscopy*, Lecture Notes in Physics (Springer, Cham, 2024).

[44] B. Mühlschlegel, Die thermodynamischen Funktionen des Supraleiters, Z. Phys. **155**, 313 (1959).

[45] R. Khasanov, R. Gupta, D. Das, A. Leithe-Jasper, and E. Svanidze, Single-gap versus two-gap scenario: Specific heat and thermodynamic critical field of the noncentrosymmetric superconductor BeAu, Phys. Rev. B **102**, 014514 (2020).

[46] G. A. Ummarino and R. S. Gonnelli, Breakdown of Migdal's theorem and intensity of electron-phonon coupling in high-T_c superconductors, Phys. Rev. B **56**, R14279(R) (1997).

[47] G. A. Ummarino, in *Emergent Phenomena in Correlated Matter*, edited by E. Pavarini, E. Koch, and U. Schollwock (Forschungszentrum Jülich GmbH and Institute for Advanced Simulations, Jülich, Germany, 2013), pp. 13.1–13.36.

[48] C. Setty, M. Baggioli, and A. Zaccone, Anharmonic theory of superconductivity in the high-pressure materials, Phys. Rev. B **103**, 094519 (2021).

[49] N. V. Nghia, H. K. Hieu, The melting curves of tin, uranium, cadmium, thallium, and indium metals under pressure, Chem. Phys. **553**, 111389 (2022).

[50] K. Takemura, Effect of pressure on the lattice distortion of indium to 56 GPa, Phys. Rev. B **44**, 545 (1991).

[51] A. Salamat, R. Briggs, P. Bouvier, S. Petitgirard, A. Dewaele, M. E. Cutler, F. Cora, D. Daisenberger, Gaston Garbarin and P. F. McMillan, High-pressure structural transformations of Sn up to 138 GPa: Angle-dispersive synchrotron x-ray diffraction study, Phys. Rev. B **88**, 104104 (2013).